

Qingyun Hu, Hsiu-Wei Cheng, Philipp Stock, Thomas Utzig, Buddha R. Shrestha, Theodoros Baimpos and Markus Valtiner\*

# ELUCIDATING THE STRUCTURE OF SOLID/ ELECTROLYTE INTERFACES

## Force probe experiments at hydrophilic, hydrophobic and electrified aqueous as well as ionic liquid | electrode interfaces

Solid electrolyte interfaces are central to reactivity, stability and self-organization in a large range of complementary fields and disciplines. It is widely appreciated, that solid|solution interfaces are central to processes involving cell-to-substrate interaction<sup>[1-3]</sup>, self-assembly and self-organization in biological and biomaterials<sup>4</sup>, stability of colloidal dispersions and electrochemical energy storage and electro-catalysis<sup>[5-6]</sup> as well as corrosion<sup>[7]</sup>.

In all of these fields understanding, predicting and controlling solid|electrolyte interfaces is of overarching importance to further advance technologic applications of even the most diametrically opposed materials used e.g. in biomedical or energy storage and energy harvesting applications. As such, the structure of solid|solution interfaces has always been appreciated as essential to interfacial interactions and reactions, yet a direct experimental probing of the atomistic structure of a solid|electrolyte interface is still one of the most challenging fields in fundamental science.

In a very generalized view, the symmetry break from an extended solid surface into an electrolyte solution leads to a variety of phenomena that can be described in terms of a *depletion* or *enrichment layer formation* away from a surface into an electrolyte. As displayed in **Figure 1**, with enrichment or depletion layer formation we refer to the transition from any bulk solid (or thin film) through a solution-side layer with increased and/or decreased concentration of solution species (water, ions, solutes) that can be well-ordered or disordered. Depletion may occur due to strong solvent|solvent or solvent|solute interactions as well as due to repulsive interactions of solutes and/or solvent molecules with a surface. Enrichment may occur e.g. due to attractive solute|surface interactions or weak solute/solvent interactions. The detailed molecular arrangement of such a solution side structuring decisively determines e.g. reaction pathways of educts and products diffusing or migrating to/away from a reactive surfaces, and/or interaction forces felt by other

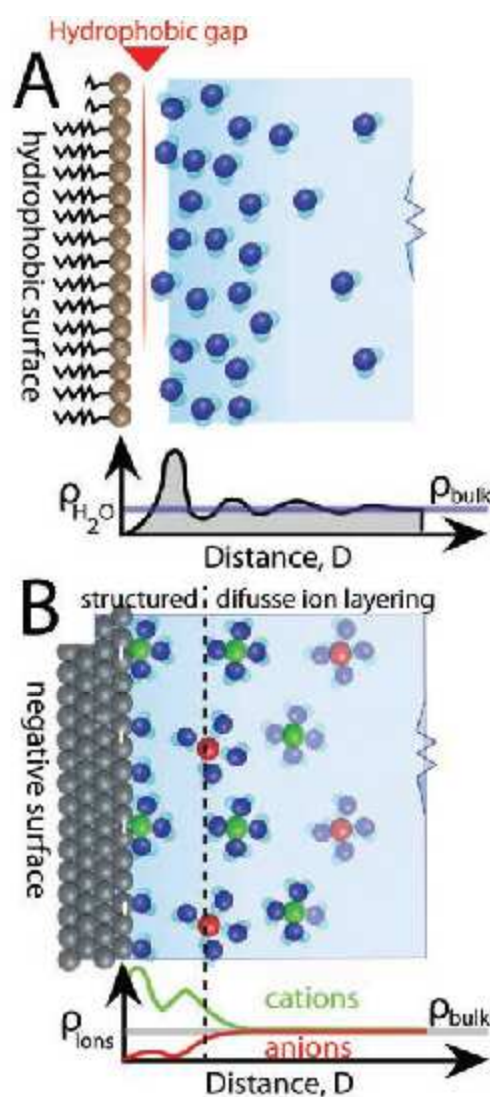


**Fig. 1.** Electrolyte structuring at (A) hydrophobic and (B) hydrophilic surfaces and typical water/ion density  $\rho$  versus distance profiles. (A) At a hydrophobic surface in aqueous solutions a small depletion layer (hydrophobic gap) of about 2-3 Å forms due to weak surface|water interactions and strong hydrogen bonding on the solution side. (B) At charged, hydrophilic and/or electrified surfaces ions of opposite charge are attracted, while ions of like charge are repelled, forming an enrichment/ depletion layer where charge neutrality is maintained. Also, at hydrophilic and/or charged surfaces water can strongly adsorb. Adsorption can be specific or non-specific, and ions may or may not strip their hydration shell depending on the overall energy balance. Also, this can lead to density variation in the ion and water layering.

Corresponding author information:

Dr. techn. Markus Valtiner  
Max-Planck-Institut f. Eisenforschung GmbH, Department for Interface  
Chemistry and Surface Engineering  
Max-Planck-Straße 1, D-40237 Düsseldorf, Germany  
Tel.: +49 211 6792447  
E-Mail: Valtiner@mpie.de

similarly structured interfaces approaching any solid|electrolyte interface e.g. during self-organisation of matter.

From a thermodynamic point of view, a subtle entropic (e.g. entropy of mixing) and enthalpic energy balance of possible chemical and physical interaction (specific and non-specific adsorption), hydrogen bonding and electrostatic attraction of solvent and solute molecules to surfaces and within the electrolyte side are directly leading to the formation of interfacial solutions-side layering up to tens of nanometers away from a solid surface. In this brief review, we will give an overview about the structuring of electrolyte solutions at (A) hydrophobic, (B) charged and (C) electrochemically polarized surfaces in aqueous solutions, as well as (D) ion layering in ionic liquids at charged and metallic surfaces. In particular, we will discuss recent advances in our understanding of interfacial water and ion structuring and its influence on interaction forces in electrolyte solutions.

Studying hydrophobic and charged solid|electrolyte interfaces has a long-standing tradition in colloid and interface science<sup>[8]</sup>, with an ever increasing success to generate molecular and fundamental insight into structure and reactivity at solid|electrolyte interfaces. Currently, the surface science community is making a significant effort and transformation aiming towards realistic environments and in particular solid|electrolyte interfaces<sup>9</sup>. As such it is an exciting time in interface science; colloid and interface scientists as well as surface scientists are converging their efforts towards the same aim – an atomistic and molecular description of solid|electrolyte interfaces. We can expect vast advances in our molecular understanding of solid|electrolyte interfaces within the next decade.

## EXPERIMENTAL TECHNIQUES FOR STUDYING SOLID|LIQUID INTERFACES

In the following, we will first provide a very brief overview on techniques that allow for a direct probing of the solid/electrolyte interface. Both interfacial spectroscopies with **non-linear optical techniques** as well as **spectroscopic ellipsometry** provide a direct view into the molecular structure and optical properties of thin films at interfaces. For instance, R. Scheu et al. could recently show that no ions adsorb to hydrophobic surfaces from NaCl based solutions<sup>[10-11]</sup>. Complementary, **synchrotron based X-ray diffraction experiments**, surface sensitive X-ray absorption fine spectroscopy (XAFS)<sup>[12]</sup>, and X-ray reflectivity experiments have been extensively used to unravel a detailed picture of the density profile and/or well-ordered (i.e. coherently diffracting) structures away from an isolated smooth and rough surfaces<sup>[13-16]</sup>. In particular, reflectivity experiments can also reveal dynamics at solid/electrolyte interfaces<sup>[17-18]</sup>. **Direct imaging with scanning probe microscopies (SPM)**, and in particular with atomic force microscopy (AFM) and scanning tunnelling microscopy (STM)<sup>[19]</sup>, provide an exciting potential for a real-space view into solvent structuring and ion adsorptions in electrolyte solutions. Here, the biggest challenge is to unambiguously determine, what exactly scanning probe microscope images detail on the molecular scale. It is extremely difficult to distinguish effects from structuring at the

probe tip and the probe surface; both are integrated simultaneously into any taken image. Considerable simulation effort and comparison to experiments is necessary to further progress to a conclusive molecular picture based on SPM imaging<sup>20</sup>.

**Force probe experiments** are an interesting and quite straightforward alternative for directly probing interfacial solvent and ion layering at any interfaces. Force probe experiments are typically performed using the two complementary techniques of force spectroscopy in an atomic force microscope<sup>[21]</sup>, or surface forces apparatus measurements<sup>[22-23]</sup>. In a typical surface force experiment two surface are approaching to distance  $D \rightarrow 0$ , the force response due to overlapping of the hydration layers gives direct information about interactive forces, and at the same time discontinuities in the force versus distance characteristics indicate stable layer formations.

In a first approximation (neglecting discontinuities due to molecular details) force versus distance profiles can be very effectively described by a linear superposition of attractive Van der Waals forces ( $F_{VDW}$ ), electric double layer forces ( $F_{EDL}$ ) and hydration layer ( $F_{Hy}$ ) dominated force contributions. Hydration effects are treated integral in terms of an exponential hydration force. Deviations from  $F_{Hy}$  will be shown and discussed below. Additionally, even roughness effects can be extended into the linear superposition concept quite effectively<sup>[24-25]</sup>, a subtlety we do not attempt to discuss in any detail here. The following equation has been used very successfully to model forces acting between a flat surfaces and a sphere of radius  $R$  during approach:

$$\frac{F}{R}(D) = F_{VDW} + F_{Hy} + F_{EDL} (+ F_{roughness} + \dots) =$$

$$\frac{A_H}{6D^2} - 4\pi Hy \cdot \gamma_{eff} e^{-\frac{D}{\lambda_{Hy}}} + \frac{\epsilon\epsilon_0}{\lambda_D} [2\Psi_1\Psi_2 e^{-(D-D_0)/\lambda_D} - (\Psi_1^2 + \Psi_2^2) e^{-2(D-D_0)/\lambda_D}] + \dots \quad [\text{N m}^{-1}] \text{ (Equation 1)}$$

with the Hamaker constant  $A_H$ , an effective hydration parameter  $Hy$ , an effective interfacial tension  $\gamma_{eff}$ , the typical decay length of hydration interactions  $\lambda_{Hy} \sim 1$  nm, the Debye screening length of the electrolyte  $\lambda_D$  and the surface potentials of the two interacting surfaces  $\Psi_1$  and  $\Psi_2$ . Here we use a constant potential solution for modelling  $F_{EDL}$ . Constant charge<sup>[8]</sup> and mixed analytical solutions (including charge regulations<sup>[26]</sup>) are available but beyond the scope of this article.  $Hy = 1$  characterizes the interaction between two fully hydrophobic surfaces, while  $Hy < 0$  characterizes repulsive hydration layering due to specific and non-specific adsorptions at the interface.  $D$  is the separation distance,  $D_H$  is the hydration force decay length,  $D_0$  allows a shift of the plane of origin of the diffuse electric double layer interaction, that may be e.g. due to a strong inner layer structuring.  $D_0$  is typically close to or equal to  $D_H$ , indicating that strong inner layer structuring switches to diffuse layering at  $D \sim D_0$ .

The first successful application of this linear superposition dates back to the well-known Derjaguin-Landau-Verwey-Overbeek theory (DLVO-theory) that considered VDW and EDL

forces acting at the same time<sup>[8]</sup>. **Equation 1** extends this concept by additional linear contribution due to hydration of interface ( $F_{Hy}$ ).

For instance, the stability of colloidal dispersions could be well predicted and rationalized in terms of the EDL based electrostatic repulsion between like particles that prevents colloids from approaching into an attractive VDW minimum<sup>[8]</sup>. In the recent years we worked intensively on extending this concept to electrified interfaces with strongly adsorbed ions and with considerable surface roughness<sup>[27-29]</sup>. Donaldson et al. unified hydration forces at hydrophobic and hydrophilic interfaces into the Hydra equation used in terms of  $F_{Hy}$  in **Equation 1**<sup>[23, 30]</sup>.

**Exemplarily, Figure 2** shows calculated forces (**Equation 1**) acting between a flat surfaces and a sphere of radius  $R$  during approach. Here, we directly compare to cases, a fully hydrophobic force versus distance characteristic with  $Hy = 1$  and a hydrophilic case with  $Hy = -0.15$ . In addition, in **Figure 2 (A)** long range electric double layer forces are set repulsive with  $\Psi_1 = 80$  mV and  $\Psi_2 = 80$  mV. Two regimes are clearly visible: First, at long range electric double layer forces dominate the force profiles for both hydrophilic and hydrophobic interfaces. At short range below about  $D \leq 5-6$  nm hydration forces lead to an attractive or repulsive regime at hydrophobic and hydrophilic surfaces, respectively. In **Figure 2 (B)** long range electric double layer forces are set attractive with  $\Psi_1 = -80$  mV and  $\Psi_2 = 80$  mV. Similarly, an electrostatic and an electrolyte-layering dominated regime are clearly visible as indicated. Interestingly, hydrophilic interfaces show an electric double layer mediated attractive minimum at separation distances of  $D \sim 4$  nm, that is overpowered by a strong repulsion at  $D \leq 4$  nm. In the following section we discuss selected examples, and discuss how this model can describe the behaviour of hydrated interfaces during approach and during interaction.

## A - ELECTROLYTE STRUCTURING AND FORCES ACROSS HYDROPHOBIC INTERFACES

As indicated in **Figure 1 (A)**, in aqueous solutions hydrophobicity leads to a depletion of water and ions away from any hydrophobic interface, giving rise to what is famously known as hydrophobic gap, where the distribution-density of water molecules and ions at the interface is minimized. For instance X-ray reflectivity measurements could show a clear decrease of the water density,  $\rho_{H_2O}$  within the first few Å (about 3-5 Å) away from hydrophobic interfaces in aqueous electrolytes<sup>[17-18]</sup>. Similarly, non-linear optical spectroscopy revealed that NaCl-ions do not adsorb to hydrophobic interfaces from aqueous solutions<sup>[10-11]</sup>.

Thermodynamically, this depletion of water at the interface is due to the strong water|water interaction compared to the relatively small interaction energy of water molecules with hydrophobic surfaces. Hydrophobic surfaces essentially only attract ions and water through Van der Waals interactions, while no specific or non-specific surfaces sites allow for hydrogen bonding between hydrophobes and water.

A direct result of this interfacial depletion layer is a strong attractive force between hydrophobic units in aqueous electrolytes, that is well-known as the so-called hydrophobic force<sup>[8, 30]</sup>. **Figure 3** shows a typical AFM force versus distance characteristic recorded during approach of two hydrophobic surfaces in aqueous solution. **Figure 3** also indicates the calculated interaction force based on a linear superposition of VDW and exponential hydrophobic forces with typical decay length of about 1 nm, indicating a good description in terms of the assumptions of **Equation 1** (e.g. linear superposition).

As can be seen directly, during approach, this hydrophobic force effectively leads to deviations from DLVO forces at  $D \sim 5-6$  nm.

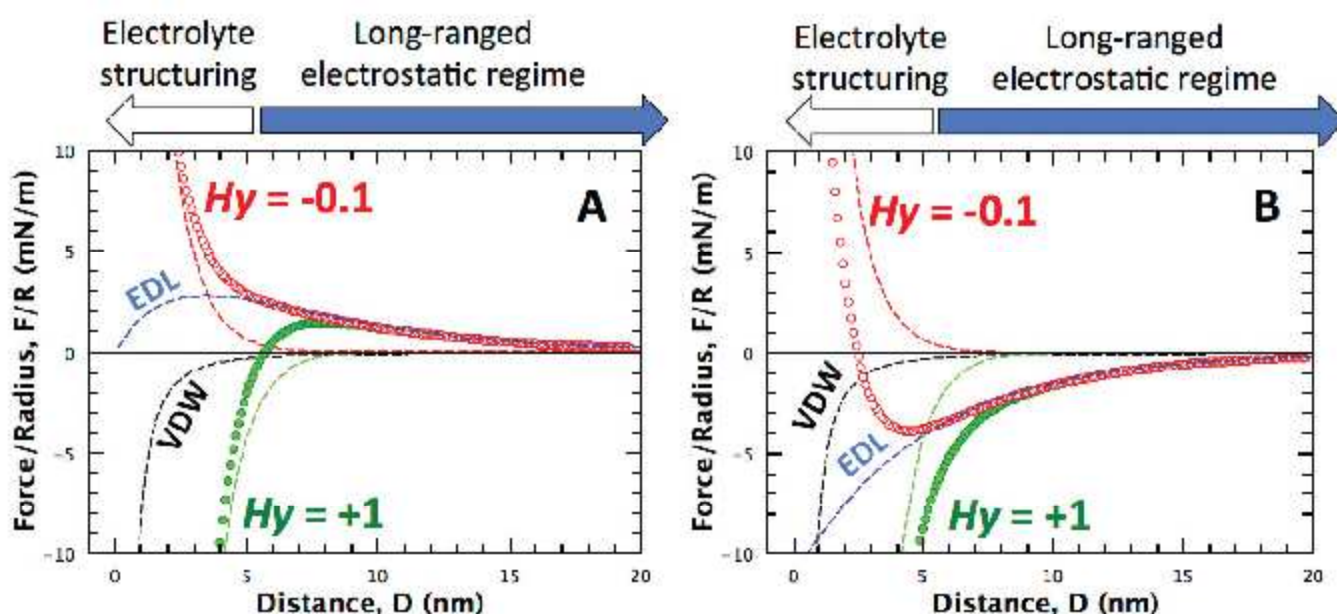


**Fig. 2.** Schematic force versus distance characteristics, composed of a linear superposition of Van der Waals (VDW), Electric double layer (EDL) and hydration forces ( $Hy$ ). Hydration forces are set to  $Hy = 1$  and  $Hy = -0.1$ , indicating attractive forces due to electrolyte depletion, and repulsive forces due to solvent/ion adsorption at hydrophobic and hydrophilic interfaces. The Debye screening length of  $\lambda_D = 5$  nm, and a Hamaker constant of  $A_H = 5 \cdot 10^{-20}$  J is used in this plot.

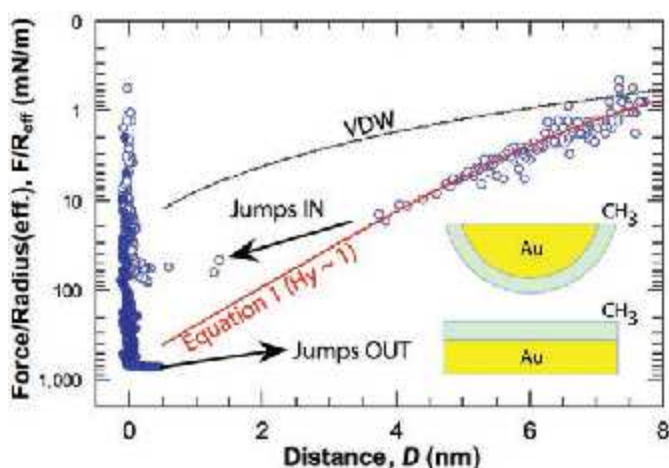


**Fig. 3.** Semi-logarithmic force versus distance profile recorded between two hydrophobic surfaces in aqueous solution at pH = 5.5 and 5 mM NaCl concentration with  $R_{\text{eff}} \sim 10\text{nm}$ . A fit to equation 1 with  $H_y \sim 1$  is shown as well. As can be seen directly from the plot, compared to acting VDW force, the hydration depletion at hydrophobic surfaces leads to an additional strong attractive force and strong adhesion upon separation.  $F_{\text{EDL}} = 0$  in this case because hydrophobic surfaces carry almost no charge.

Hence, the hydrophobic force is quite long ranged (10 s of molecular water diameters) and as such it plays an essential role in protein folding and aggregation of hydrophobic and amphiphilic molecules in water (lipid-bilayer formations). It may also be important in technological applications, where wetting/de-wetting and controlled aggregation of hydrophobes are critical.

In the future, force probe experiments will provide further detailed insight into hydrophobic interactions, and in particular high salt concentrations and specific influence of dissolved ions on hydrophobic forces. Of particular interest will also be the influence of the size of hydrophobic units on hydrophobic interactions. E.g. small hydrophobes such as methane can be effectively enclosed into water structures based on enthalpic energy gains<sup>[31-32]</sup>, which prevents direct harvesting of methane-ice reservoirs. Salt and additives can directly affect hydrophobic forces and may provide interesting strategies for an economic harvesting of these abundant natural resources.

## B - STRUCTURING AND ELECTRIC DOUBLE LAYER FORCES AT CHARGED INTERFACES

Conversely to hydrophobic interfaces, and as shown in **Figure 1(B)**, charging of surfaces in electrolyte solutions leads to the formation of the so-called electric double layer, where oppositely charged ions and dipolar water molecules are attracted/ adsorbed to any charged surface. Frequently observed charging mechanisms in electrolytes include protonation/ deprotonation of surface species, electrochemical polarization<sup>[28-29]</sup> or selective dissolution of charged surface species.

**Figure 4** shows a semi-logarithmic plot of the interaction forces between two mica surfaces in hydrochloric acid at pH 4 and 1, as well as 100 mM LiCl and CsCl solutions at pH = 5. The zero distance ( $D = 0$ ) is defined as the distance between two dry mica surfaces in dry argon under high load. Under these conditions, only a single layer of  $\text{K}^+$  ions separates the two mica surfaces. In

solution the  $\text{K}^+$  ions dissolve and a mica surface obtain a maximum negative charge density of half a monolayer. This amounts to a charge density of about  $0.2\text{ C/cm}^2$ , or a surface potential of 471 mV obtained from Grahame's equation in pure water. This surface charge is balanced at the interface by the formation of an equally but oppositely charged EDL, which gives rise to the measured interaction forces. **Figure 4(A/B)** reveals several subtle information such as shifts of the force distance characteristics, strong variation of the diffuse double layer, oscillatory behaviour within the hydration layer (discrete inner layer hydration layer effects), and significant differences in the adhesion forces measured during separation (not discussed here).

In **Figure 4(A)** long range EDL forces are visible only in hydrochloric acid at pH = 3. At this pH the mica surfaces are charged negative. This negative surface charge is compensated by the formation of an EDL consisting entirely of protons. Forces can be modelled well in this case using only VDW and EDL forces with the experimental Debye length of 9.6 nm. Interestingly, no hydration forces are detectable in proton based solutions, surfaces directly approach to  $D = 0$ . This indicates, that protons do not form any significant hydration layering. This is consistent with the fact that protons do not carry any hydration shell with them.

In contrast, in hydrochloric solution at pH = 1, the force distance profile is considerably shifted out and also shifted to higher forces. This pH is well below the point of zero charge (PZC) at pH = 2.5, and the used mica surfaces are protonated and charged positively. Hence, anions are attracted towards the interface. The Debye length at pH = 1 is a much less than one nm, and hence EDL forces can not explain the observed almost exponential long range repulsive regime with  $\lambda_{\text{D}} \sim 2.5\text{ nm}$ . Clearly, hydrated anions adsorb to the positively charged mica interface and give rise to hydration forces between the two approaching surfaces. Additionally, the approach curve significantly deviates from a pure exponential force increase, indicating a layering of the anion species.

If LiCl or CsCl salts (same chloride anions) are added to the solutions at pH values above the point of zero charge of 2.5, force versus distance characteristics change dramatically (**see Figure 4 (B)**). First, the long-range component is suppressed due to the decreased Debye length. Second, in confinement the weakly hydrated  $\text{Cs}^+$  ions condensate into the mica-lattice screening the entire surface charge within the Stern layer. No EDL force is detectable in 100 mM CsCl solutions<sup>[33]</sup>. In contrast, strongly hydrated  $\text{Li}^+$  ions only partially compensate the surface charge within the Stern layer, leading to the formation of a diffuse outer double layer with DLVO behavior as indicated in **Figure 4(B)**. This is consistent with a strong binding of water to the  $\text{Li}^+$  ions that cannot specifically adsorb to mica.  $\text{Cs}^+$  on the other hand bind water weakly, and hence may exothermically condensate into the lattice of mica. This is also the reason why mica-like materials are well known and technically used as Cs-absorbers (feeding additives) in milk-production since the radioactive fall out from Chernobyl in the 1980 s. This is a clear example, where a subtle balance between hydration energies and adsorption energies dominate the resulting surface layering. As such, both LiCl and CsCl solutions exhibit oscillatory ion-hydration forces at surface separations from 2.2 nm to 4.8 Å marked with arrows in **Figure 4(A) and (B)**<sup>[33]</sup>.

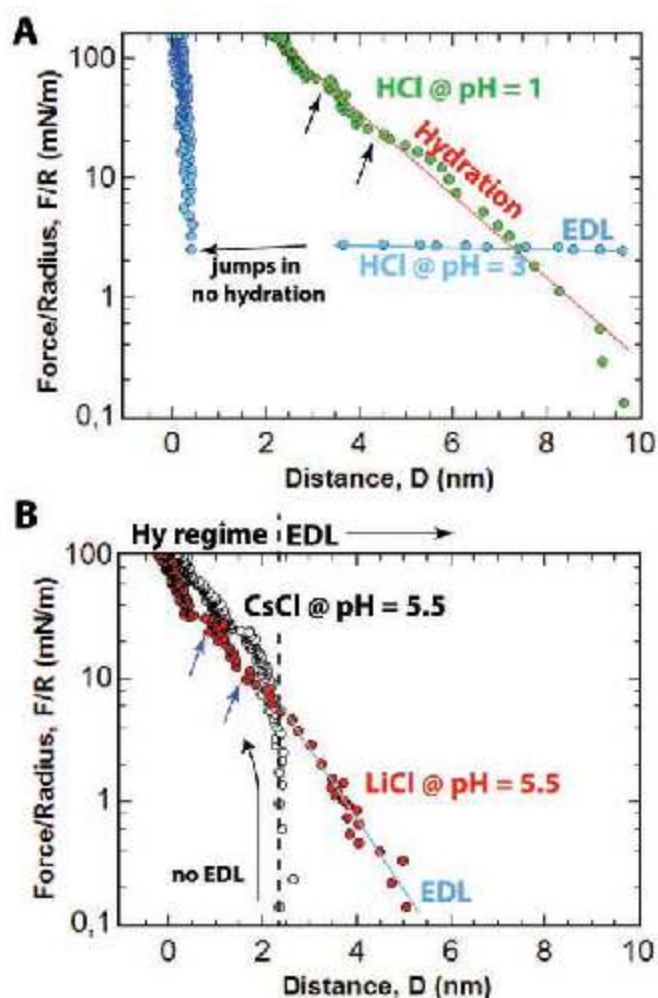


Fig. 4. Characteristic force distance profiles during approach between two Mica(0001) surfaces in (A) hydrochloric acid at pH = 1 and pH = 3 as indicated, and (B) at pH = 5.5 in 100 mM CsCl and LiCl solutions as indicated. EDL and hydration forces regimes are indicated. Arrows are also indicating discontinuities and deviations from a linear behaviour.

### C - STRUCTURING AND FORCES AT ELECTRIFIED INTERFACES IN AQUEOUS SOLUTIONS

Applying a potential at a metallic or semi-conducting interface leads to a considerable change of the surface charge, and as such directly effects the layering of electrolytes at electrified interfaces. In the last few years we have developed electrochemical cells and attachments for both Surface Forces Apparatus (SFA) and Atomic Force Microscopy (AFM), and measured the influence of surface hydration on interactions forces and ion-layering in-situ<sup>[28-29]</sup>.

**Figure 5** shows a set of characteristic force versus distance profiles measured between electrochemically polarized (from -150 mV to 800 mV vs the potential of zero charge) gold surfaces and amine terminated self-assembled monolayers on gold in 1 mM HNO<sub>3</sub> at pH = 3, using the SFA.

The plotted approach curves show two distinctly different force regimes: At separation distance,  $D$ , ranging from 40 nm to about 4 nm, the data shows the long-ranged electric dou-

ble layer force which is attractive for electrochemical potentials below the PZC and repulsive above the PZC. This interfacial force profile is consistent with the surface chemistry at the apposing interfaces. The surface terminating amine head group of the 3-aminopropyl-triethylsilane monolayer (APTES) coated mica surface is charged positively at the experimental pH value of pH = 3, while the surface potential of the gold electrode was modulated in situ using the electrochemical setup. At separation distance,  $D$ , below 4 nm, the force runs in **Figure 5** indicate an additional exponential repulsive force contribution due to hydration forces arising from the confinement of hydrated ions and water between the two apposing surfaces. The shift of the hard wall above the potential of zero charge is indicated.

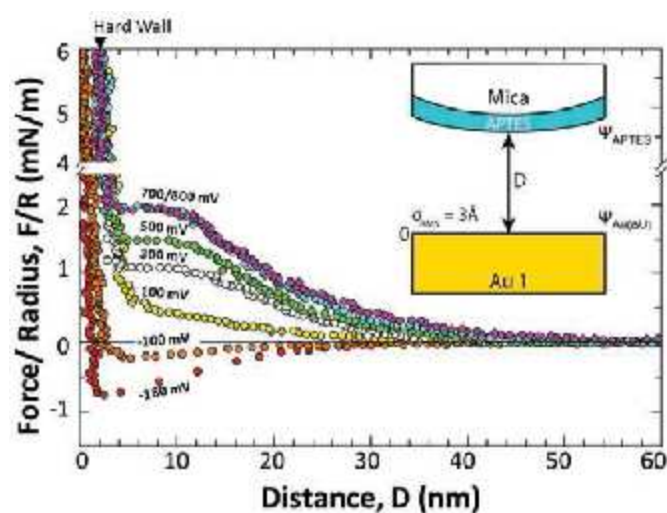


Fig. 5. Typical force–distance profiles measured during approach of opposing gold and APTES coated mica surfaces measured as function of the externally applied electrochemical potentials for an atomically smooth gold surface. The external applied potentials  $\Delta U$  ( $\Delta U = U - U_{PZC}$ ) are color-coded, and positions of the hard walls are indicated. In force spectroscopy it is convenient to reference potentials against the potential of zero charge, where the overall surface charge switches from positive to negative.

### D - STRUCTURING AND FORCES AT IONIC LIQUIDS | METAL ELECTRODE INTERFACES

Quite in contrast to aqueous or organic electrolytes with dissolved ionic salts, so-called ionic liquids (ILs) are room-temperature liquids that are composed entirely and solely of bulky organic cations and anions. ILs constitute solvents/electrolytes with very peculiar and promising properties such as a wide window of electrochemical and thermal stability among many others. As such and based on the vast potential for fine tuning structure and properties through organic synthesis, ILs have emerged as promising candidates for applications in batteries, super capacitors and e.g. solar cells to name but a few.

At electrified and charged interfaces ILs show a very interesting surface layering that is directly accessible to force probe experiments. **Figure 6** shows force versus distance characteristic at a ceramic (Mica) and a metal (Pt) surface measured with AFM. The same AFM tip was used to probe both surfaces in order to minimize tip radii effects. It is apparent, that the two surfaces form completely different layering at distances

$D \leq 10\text{--}15 \text{ \AA}$ . The final layer on Platinum surfaces shown in **Figure 6(A)** has a thickness of about  $5.3 \text{ \AA}$ , while the final layer on mica surfaces probed in **Figure 6(B)** has a thickness of about  $8.1 \text{ \AA}$ .

Comparing the forces during the typically observed instabilities with **Figures 4 and 5**, the actual interaction energy of ILs at charged interfaces seems to be weaker compared to ion adsorption in aqueous electrolytes. This constitutes another advantage of ILs over traditional electrolytes, as the ions will not interfere strongly with interfacial reactions by blocking active sites by strong adsorption they can readily be replaced. An exact structure can unfortunately not be ascertained at this point in time, as the actual molecular structure is not probed here. In this direction molecular modelling may help to further understand the detailed molecular arrangements.

In typical battery fluids the interfacial solvent layering of ILs and/or organic electrolytes controls e.g. transition state barrier during charging and discharging of a battery, including in particular the formation of the solid-electrolyte interface that controls performance and lifetime of a rechargeable battery. In general, and as can be seen in **Figure 6** layering of ILs at electrified interfaces is observed up to 4-5 nm distance. Considering the typical size of IL constituents (about  $5 \text{ \AA} \approx 1 \text{ nm}$ ) this amounts to only about 4-5 molecular layers. As such, the inner layer ordering effect in ILs is a bit less far reaching compared to layering observed in aqueous solutions that typically extends to 2-3 nm in the structured inner hydration layer.

In addition, our recent force-probe experiments with the SFA revealed that ionic liquids might not be viewed as an infinitely concentrated solution of cations and anions<sup>[27]</sup>. Quite in contrast, ionic liquids behave as effectively neutral dielectric network of cations and anions containing a concentration of about  $\sim 0.1 \text{ mM}$  of dissociated cations and anions, similar to a dilute electrolyte. As such, forces in ionic liquids show a strong inner surface layering, with a weak additional long-ranged force from overlapping diffuse double layers, which is conceptually similar to a space charge region in a semi-conductor.

## SUMMARY

We showed and discussed the large variety of interfacial ion and solvent structuring at solid|electrolyte interfaces. In summary, protons do not form hydration layers, but protonation can lead to strong anions layering. Cation layering strongly depends on the hydration energies of the involved ions. Bind-

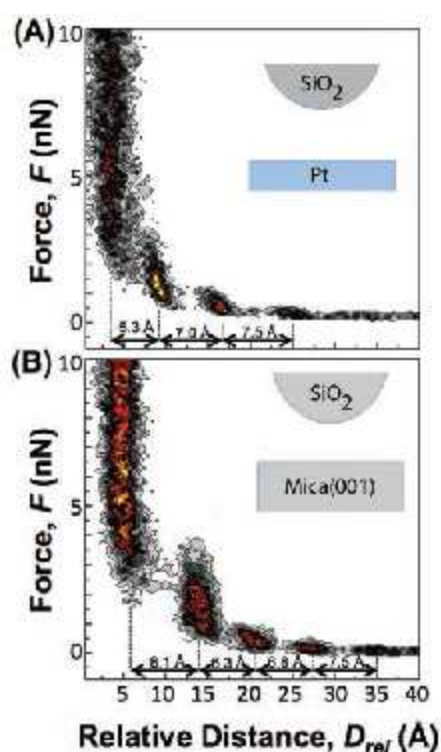


**Fig. 6.** AFM force versus distance characteristics during approach of (A) platinum surfaces and silica AFM tips, and (B) Mica surfaces and silica AFM tips measured across the ionic liquid EMIM Tf<sub>2</sub>N. Here, a 2D population mapping was applied to analyse AFM results. In total, 40 force runs were used to generate a population density map of force versus relative distance with bin sizes of (10 pN for the force, and 0.5 Å for the distance). The same AFM tip ( $R_{\text{eff}} \sim 20 \text{ nm}$ ) was used for probing both (A) platinum and (B) mica surfaces in order to minimize specific probe effects. The labelled distances inside the figures indicate the thickness of different layers.

ing energies in ILs seem much weaker compared to ion binding in aqueous solutions. From the selected examples it is apparent, how a subtle balance between adsorption, solvent-solvent, ion-solvent and ion-surface energies directly steer and control interfacial structuring and resulting interactive forces at solid|liquid interfaces.

As such, force probe experiments provide a unique and complementary view into both the structuring of electrolyte and interaction forces during approach and separation of surfaces in aqueous and non-aqueous liquids. This is an aspect that other interface sensitive techniques can not probe directly interactive forces and dynamic structure/property responses are accessible directly and uniquely in force probe experiments<sup>[34]</sup>.

As a conclusive remark we want to emphasise that all of the techniques we mentioned in our experimental section above, as well as force probe experiments, provide unique pieces of the puzzle that will allow us to advance our molecular understanding of interfaces at steady-state and during active (interacting) conditions. However, high level theory such as molecular dynamics<sup>[35]</sup> or neural networks<sup>[36]</sup>, and *ab initio* calibrated molecular dynamics<sup>[37]</sup> will play an important role as an integrative tool in linking results and data of interfacial experimental techniques to an actual and conclusive molecular and dynamic picture of an interface.

## ACKNOWLEDGEMENTS

The German research foundation (DFG) is acknowledged from M.V., T. U. and P. S for support though funding in the framework of a Materials World Network (Project number: VA 689/3-1). Also, M.V. and Q.H. gratefully acknowledge funding of DFG through the cluster of excellence RESOLV (Projectcode EXC 1069). H.-W. C. and T.U. gratefully acknowledge funding from IMPRS-SURMAT. M.V. gratefully acknowledges a research stipend from the Max-Buchner-Stiftung of the DECHEMA.

## REFERENCES

- [1] Arlett, J. L.; Myers, E. B.; Roukes, M. L., Comparative Advantages of Mechanical Biosensors. *Nature Nanotechnology* 2011, **6** (4), 203-215.
- [2] Malanchi, I.; Santamaria-Martinez, A.; Susanto, E.; Peng, H.; Lehr, H.-A.; Delaloye, J.-F.; Huelsenken, J., Interactions between Cancer Stem Cells and Their Niche Govern Metastatic Colonization. *Nature* 2012, **481** (7379), 85-95.

- [3] Trappmann, B.; Gautrot, J. E.; Connelly, J. T.; Strange, D. G. T.; Li, Y.; Oyen, M. L.; Stuart, M. A. C.; Boehm, H.; Li, B.; Vogel, V.; Spatz, J. P.; Watt, F. M.; Huck, W. T. S., Extracellular-Matrix Tethering Regulates Stem-Cell Fate. *Nature Materials* 2012, **11** (7), 642-649.
- [4] Lee, B. P.; Messersmith, P. B.; Israelachvili, J. N.; Waite, J. H., Mussel-Inspired Adhesives and Coatings. *Annual review of materials research* 2011, **41**, 99-132.
- [5] Mayrhofer, K. J. J.; Juhart, V.; Hartl, K.; Hanzlik, M.; Arenz, M., Adsorbate-Induced Surface Segregation for Core-Shell Nanocatalysts. *Angewandte Chemie-International Edition* 2009, **48** (19), 3529-3531.
- [6] Stamenkovic, V. R.; Mun, B. S.; Arenz, M.; Mayrhofer, K. J. J.; Lucas, C. A.; Wang, G.; Ross, P. N.; Markovic, N. M., Trends in Electrocatalysis on Extended and Nanoscale Pt-Bimetallic Alloy Surfaces. *Nature Materials* 2007, **6** (3), 241-247.
- [7] Frankel, G. S., Pitting Corrosion of Metals. *Journal of The Electrochemical Society* 1998, **145** (6), 2186-2198.
- [8] Israelachvili, J., *Intermolecular and Surface Forces*. Elsevier: 2010; Vol. Third Edition.
- [9] Grass, M. E.; Karlsson, P. G.; Aksoy, F.; Lundqvist, M.; Wannberg, B.; Mun, B. S.; Hussain, Z.; Liu, Z., New Ambient Pressure Photoemission Endstation at Advanced Light Source Beamline 9.3.2. *Review of Scientific Instruments* 2010, **81** (5) 053106.
- [10] Scheu, R.; Chen, Y.; Subinya, M.; Roke, S., Stern Layer Formation Induced by Hydrophobic Interactions: A Molecular Level Study. *Journal of the American Chemical Society* 2013, **135** (51), 19330-19335.
- [11] Scheu, R.; Rankin, B. M.; Chen, Y.; Jena, K. C.; Ben-Amotz, D.; Roke, S., Charge Asymmetry at Aqueous Hydrophobic Interfaces and Hydration Shells. *Angewandte Chemie* 2014, Int. Ed., **53** (36), 9560-9563.
- [12] Keil, P.; Lutzenkirchen-Hecht, D.; Frahm, R., Selective Study of Atoms in Rough Surfaces by Means of Off-Specular Grazing Incidence Xafs. *Europhysics Letters* 2005, **71** (1), 77-83.
- [13] Fenter, P.; Sturchio, N. C., Mineral-Water Interfacial Structures Revealed by Synchrotron X-Ray Scattering. *Progress in Surface Science* 2004, **77** (5-8), 171-258.
- [14] Mezger, M.; Reichert, H.; Schoeder, S.; Okasinski, J.; Schroeder, H.; Dosch, H.; Palms, D.; Ralston, J.; Honkimaki, V., High-Resolution in Situ X-Ray Study of the Hydrophobic Gap at the Water-Octadecyl-Trichlorosilane Interface. *Proceedings of the National Academy of Sciences of the U. S. A.* 2006, **103** (49), 18401-18404.
- [15] Mezger, M.; Sedlmeier, F.; Horinek, D.; Reichert, H.; Pontoni, D.; Dosch, H., On the Origin of the Hydrophobic Water Gap: An X-Ray Reflectivity and Md Simulation Study. *Journal of the American Chemical Society* 2010, **132** (19), 6735-6741.
- [16] Poynor, A.; Hong, L.; Robinson, I. K.; Granick, S.; Zhang, Z.; Fenter, P. A., How Water Meets a Hydrophobic Surface. *Physical Review Letters* 2006, **97**, 266101.
- [17] Mezger, M.; Ocko, B. M.; Reichert, H.; Deutsch, M., Surface Layering and Melting in an Ionic Liquid Studied by Resonant Soft X-Ray Reflectivity. *Proceedings of National Academy of Sciences of the U. S. A.* 2013, **110** (10), 3733-3737.
- [18] Mezger, M.; Schroder, H.; Reichert, H.; Schramm, S.; Okasinski, J. S.; Schoder, S.; Honkimaki, V.; Deutsch, M.; Ocko, B. M.; Ralston, J.; Rohwerder, M.; Stratmann, M.; Dosch, H., Molecular Layering of Fluorinated Ionic Liquids at a Charged Sapphire (0001) Surface. *Science* 2008, **322** (5900), 424-428.
- [19] Magnussen, O. M., Ordered Anion Adlayers on Metal Electrode Surfaces. *Chemical Reviews* 2002, **102** (3), 679-725.
- [20] Kawai, S.; Foster, A. S.; Canova, F. F.; Onodera, H.; Kitamura, S.; Meyer, E., Atom Manipulation on an Insulating Surface at Room Temperature. *Nature communications* 2014, **5**, 4403.
- [21] Israelachvili, J., Differences between Non-Specific and Bio-Specific, and between Equilibrium and Non-Equilibrium, Interactions in Biological Systems. *Q. Rev. Biophys.* 2005, **38**, 331-337.
- [22] Valtiner, M.; Donaldson, S. H., Jr.; Gebbie, M. A.; Israelachvili, J. N., Hydrophobic Forces, Electrostatic Steering, and Acid-Base Bridging between Atomically Smooth Self-Assembled Monolayers and End-Functionalized Pegolated Lipid Bilayers. *Journal of the American Chemical Society* 2012, **134** (3), 1746-1753.
- [23] Donaldson, S. H., Jr.; Royne, A.; Kristiansen, K.; Rapp, M. V.; Das, S.; Gebbie, M. A.; Lee, D. W.; Stock, P.; Valtiner, M.; Israelachvili, J., Developing a General Interaction Potential for Hydrophobic and Hydrophilic Interactions. *Langmuir : the ACS journal of surfaces and colloids* 2014 Aug 20th.
- [24] Valtiner, M.; Kristiansen, K.; Greene, G. W.; Israelachvili, J. N., Effect of Surface Roughness and Electrostatic Surface Potentials on Forces between Dissimilar Surfaces in Aqueous Solution. *Advanced Materials* 2011, **23** (20), 2294-2298.
- [25] Valtiner, M.; Grundmeier, G., Single Molecules as Sensors for Local Molecular Adhesion Studies. *Langmuir* 2010, **26** (2), 815-820.
- [26] Tabor, R. F.; Wu, C.; Grieser, F.; Dagastine, R. R.; Chan, D. Y. C., Measurement of the Hydrophobic Force in a Soft Matter System. *Journal of Physical Chemistry Letters* 2013, **4** (22), 3872-3877.
- [27] Gebbie, M. A.; Valtiner, M.; Banquy, X.; Fox, E. T.; Henderson, W. A.; Israelachvili, J. N., Ionic Liquids Behave as Dilute Electrolyte Solutions. *Proceedings of National Academy of Sciences of the U. S. A.* 2013, **110** (24), 9674-9679.
- [28] Valtiner, M.; Anka, G. N.; Bashir, A.; Renner, F. U., Atomic Force Microscope Imaging and Force Measurements at Electrified and Actively Corroding Interfaces: Challenges and Novel Cell Design. *Review of Scientific Instruments* 2011, **82** (2), 023703.
- [29] Valtiner, M.; Banquy, X.; Kristiansen, K.; Greene, G. W.; Israelachvili, J. N., The Electrochemical Surface Forces Apparatus: The Effect of Surface Roughness, Electrostatic Surface Potentials, and Anodic Oxide Growth on Interaction Forces, and Friction between Dissimilar Surfaces in Aqueous Solutions. *Langmuir : the ACS journal of surfaces and colloids* 2012, **28** (36), 13080-13093.
- [30] Donaldson, S. H., Jr.; Lee, C. T., Jr.; Chmelka, B. F.; Israelachvili, J. N., General Hydrophobic Interaction Potential for Surfactant/Lipid Bilayers from Direct Force Measurements between Light-Modulated Bilayers. *Proceedings of National Academy of Sciences of the U. S. A.* 2011, **108** (38), 15699-15704.
- [31] Hammer, M. U.; Anderson, T. H.; Chaimovich, A.; Shell, M. S.; Israelachvili, J., The Search for the Hydrophobic Force Law. *Faraday Discussions* 2010, **146**, 299-308.
- [32] Chaimovich, A.; Shell, M. S., Tetrahedrality and Structural Order for Hydrophobic Interactions in a Coarse-Grained Water Model. *Physical Review E* 2014, **89** (2) 022140.
- [33] Baimpos, T.; Shrestha, B. R.; Raman, S.; Valtiner, M., Effect of Interfacial Ion Structuring on Range and Magnitude of Electric Double Layer, Hydration, and Adhesive Interactions between Mica Surfaces in 0.05-3 M Li(+) and Cs(+) Electrolyte Solutions. *Langmuir* 2014, **30** (15), 4322-32.
- [34] Shrestha, B. R.; Baimpos, T.; Raman, S.; Valtiner, M., Angstrom-Resolved Real-Time Dissection of Electrochemically Active Noble Metal Interfaces. *ACS nano* 2014, **8** (6), 5979-87.
- [35] Martinez-Suarez, L.; Frenzel, J.; Marx, D., Cu/Zn Nanocatalysts in Response to Environmental Conditions: Surface Morphology, Electronic Structure, Redox State and Co2 Activation. *Physical chemistry chemical physics : PCCP* 2014, **16** (47), 26119-26136.
- [36] Behler, J., Representing Potential Energy Surfaces by High-Dimensional Neural Network Potentials. *Journal of Physics-Condensed Matter* 2014, **26** (18), 183001.
- [37] Wiebe, J.; Spohr, E., Double Layer Effects in a Model of Proton Discharge on Charged Electrodes. *Beilstein Journal of Nanotechnology* 2014, **5**, 973-982.

Katrin R. Siefertmann

# DYNAMICS AT THE LIQUID - VACUUM INTER-FACE PROBED BY PICOSECOND TIME-RESOLVED PHOTOELECTRON SPECTROSCOPY

Ultrafast time-resolved spectroscopy is an indispensable tool to study fundamental processes in gas phase, liquids and solids. Among the multitude of studied phenomena, ultrafast dynamics in water remain a topic of high scientific interest. This interest is mainly owed to the unique properties of water and its general importance for life on earth. As many processes in water do not proceed in the bulk but at the interfaces of water with solid materials (e.g. with semiconductors [1]), soft matter (e.g. biological tissue [2]), or gas phases (e.g. in atmospheric chemistry [3]), water interfaces increasingly move into the focus of scientific investigations. Here, I present an emerging experimental tool to monitor fundamental dynamics at the liquid water/vacuum interface: Picosecond (ps) time-resolved photoelectron spectroscopy on liquid microjets [4, 5]. Key is that photoelectron spectroscopy is a surface sensitive technique. By suitable adjustment of experimental parameters the detected photoelectrons exclusively originate from within the first few nanometers from the liquid surface. This aspect renders it a unique tool for the investigation of surface dynamics. This article presents (1) main aspects of the experimental setup for picosecond time-resolved photoelectron spectroscopy on liquids. It further highlights how this experimental approach has answered fundamental questions on (2) the ultrafast expansion dynamics of supercritical water into vacuum [6-8] and (3) the binding energy of solvated electrons in liquid water [9, 10].

## 1. PICOSECOND TIME-RESOLVED PHOTOELECTRON SPECTROSCOPY ON A LIQUID MICROJET: ADVANTAGES AND EXPERIMENTAL CHALLENGES

Photoelectron spectroscopy measures electron binding energies of the system under investigation. This allows interesting insights into its electronic structure, while time-resolved experiments allow to map changes of this electronic structure as a function of time; i.e. in response to an external stimuli (e.g. optical excitation). Time-resolved photoelectron spectroscopy is thus a powerful method for the investigation of ultrafast processes in atoms, molecules and condensed matter. In these experiments an ultrashort laser pulse, the so-

called pump-pulse, excites the system under investigation. Subsequent dynamics of this excited system are monitored with a second ultrashort laser pulse (probe-pulse), which photoionizes the sample. Photoelectrons are detected and the change of photoelectron signal as a function of the temporal delay between pump- and probe-pulse reveals the dynamics of the excited system. This section describes the experimental challenges of time-resolved photoelectron spectroscopy on a liquid microjet and the unique advantages with regard to the investigation of dynamics at the liquid surface. The major experimental challenges are summarized by the following two questions: a) How to create high energy photons in ultrashort pulses of light? b) How to handle a liquid (in particular liquid water) in high vacuum?

a) A major challenge of ultrafast time-resolved photoelectron spectroscopy is that such experiments require high energy photons in ultrashort pulses of light. Short pulses of light with femtosecond ( $1 \text{ fs} = 1 \times 10^{-15} \text{ s}$ ) duration are required in order to capture the ultrafast fundamental processes in atoms, molecules and condensed matter. High photon energies are required for the photoionization of the sample with the probe-pulse. In many cases the excited states (which are prepared by the pump-pulse) can already be photoionized with photon energies of about 5 - 6 eV. This experimental approach is termed time-resolved two-photon-photoemission (2PPE) spectroscopy and the required photon energies are accessible via frequency mixing processes of femtosecond laser pulses [11, 12]. However, higher photon energies are needed to photoionize the valence states of the system under investigation. In the case of water, photon energies of about 40 eV are required in order to record a photoelectron spectrum with signals from all valence states. Such high energy photons in ultrashort pulses of light only became accessible within the last decade with the advent and development of two new types of light sources: a) Free-electron lasers and b) light sources based on high-harmonic-generation (HHG) (see figure 1). To date, numerous time-resolved photoelectrons spectroscopy experiments with both approaches have been reported (see e.g. Ref. [13, 14]). In particular, HHG also makes pulses of light with attosecond ( $1 \text{ as} = 1 \times 10^{-18} \text{ s}$ ) duration accessible which can be used to measure sub- and few-femtosecond short dynamics [15].

b) Photoelectron spectroscopy requires a sample in high vacuum in order to avoid scattering processes of outgoing photoelectrons with gas phase molecules. This constitutes a challenge

---

Dr. Katrin Siefertmann  
Leibniz-Institute of Surface Modification (IOM)  
Permoserstr. 15, D-04318 Leipzig, Germany  
Tel.: +49 (0)341 235- 3364  
E-Mail: katrin.siefertmann@iom-leipzig.de

for experiments on liquids, since volatile liquids will rapidly evaporate and freeze in high vacuum. Photoelectron studies on pure volatile liquids thus only became feasible with the emergence of the liquid microjet technique [16]. Since then, several photoelectron spectroscopy experiments on pure liquids and on various solutions have been performed with synchrotron light sources [17, 18].

Figure 1 illustrates how our experimental setup combines high-harmonic generation (HHG) and liquid microjet technology in vacuum for picosecond time-resolved photoelectron spectroscopy experiments on liquids [4-6]. In our setup, the output of a femtosecond laser system is split into pump- and probe-pulse. We guide the pump-pulse over a delay stage, which is used to set the temporal delay between the arrival of the pump- and probe-pulse at the sample. The pump-pulse is further sent into a wavelength tuning unit in which frequency mixing processes allow to adapt the wavelength of the pump-pulse to the experimental requirements. The pump-pulse then enters the vacuum chamber and is focussed onto the liquid jet sample. The probe-pulse is focussed into a capillary with rare gas (here: argon). When the intense laser field interacts with the medium, different strong field effects take place. One of these effects is high-harmonic generation, which results in high-energetic photons featuring odd multiples of the fundamental photon energy. In our experimental setup, a toroidal reflection grating spatially separates these discrete harmonics, and is aligned such that either the 25th (~39 eV) or 27th (~42 eV) harmonic is focussed onto the sample. The probe-pulse photoionizes the sample and photoelectrons are detected with a time-of-flight photoelectron spectrometer.

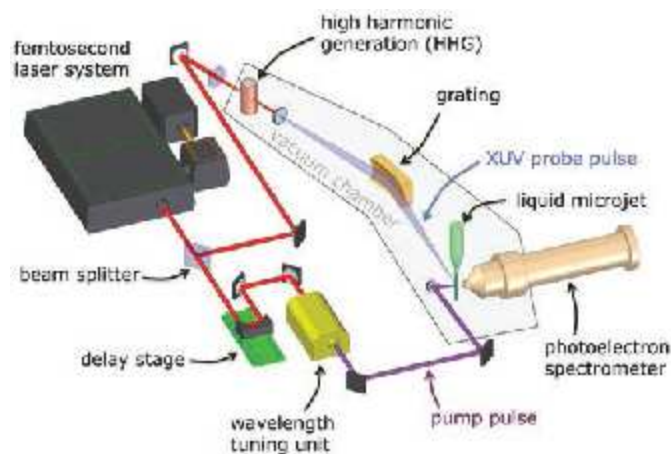


**Fig. 1:** Schematic representation of the experimental setup for picosecond time-resolved photoelectron spectroscopy on liquid surfaces.

Photoelectron spectroscopy is a surface sensitive technique and thus particularly suited for the investigation of surfaces and surface dynamics. The reason for the surface sensitivity are inelastic scattering events which limit the escape depth of photoelectrons. In general, the probing depth is defined by the electron attenuation length (EAL). The EAL is the (shortest) distance from a starting point A to an arrival point B, at which the initial photoelectron signal  $I_0$  is reduced to  $I = I_0/e$  as a result of scattering events. Only photoelectrons generated within this distance to the material surface significantly contribute to

the structured part of the photoelectron spectrum. In the case of a liquid water sample, recent liquid jet experiments suggest an EAL on the order of 1 nm for photoelectron kinetic energies below 100 eV [19, 20]. Assuming a thickness of about 0.3 nm per liquid water monolayer [21], this corresponds to a few layers of water only and makes photoelectron spectroscopy on liquid water particularly surface sensitive (in the case of photoelectron kinetic energies < 100 eV).

Taken together, the strengths of time-resolved photoelectron spectroscopy on liquid microjets, performed with the experimental setup depicted in figure 1, are: (1) The experiment measures electron binding energies and their (pump-pulse induced) changes with a temporal resolution of < 1 ps. (2) The surface sensitivity confines the measurement to an observation window within a few nanometers from the surface. The combination of these two points renders time-resolved photoelectron spectroscopy an exquisite and unique tool to study dynamic processes at the liquid - vacuum interface.

The following two sections describe two of our major research results: A nanoscale picture of the ultrafast expansion dynamics of supercritical water into vacuum, and the determination of the binding energy of solvated electrons in liquid water.

## 2. ULTRAFAST EXPANSION DYNAMICS OF SUPERCRITICAL WATER

When femtosecond laser pulses interact with liquid water, extreme states of matter can be created. In this experiment we use a femtosecond laser pulse with a central wavelength of 2900 nm to resonantly excite the OH stretch vibration of water molecules in liquid water [6]. In good approximation, this excitation instantaneously transfers the liquid into a state with a temperature of about 1000 K and a pressure above 1 GPa; however without breaking molecular bonds or creating plasma. With the experimental approach outlined above, we were able to monitor the subsequent picosecond expansion dynamics of the hot water phase into vacuum. Unique to this experiment is, that the surface sensitivity of photoelectron spectroscopy allows to selectively monitor the expansion of the first few surface layers of water. This experiment delivered unprecedented insights into the expansion mechanisms of a supercritical water phase into vacuum and the associated timescales.

Ref. [6] describes the setup and parameters of this experiment in detail. Briefly, an optical parametric amplifier (TOPAS) and an additional frequency mixing unit transform the fundamental laser pulses ( $\lambda_c = 800$  nm) into the desired pulses with  $\lambda_c = 2900$  nm (pulse length = 250 fs,  $\sim 20$   $\mu$ J/pulse at sample position). The high absorption coefficient of liquid water at 2900 nm allows to deposit a large amount of energy into the system. In our experiment this energy is deposited within the short time of 250 fs (puls length of pump-pulse) during which the system cannot significantly expand. The result is a hot water phase with a temperatures of about 1000 K and a pressure  $p > 1$  GPa. This phase is supercritical, as the critical point of water is at  $T = 647$  K and  $p = 22$  MPa.

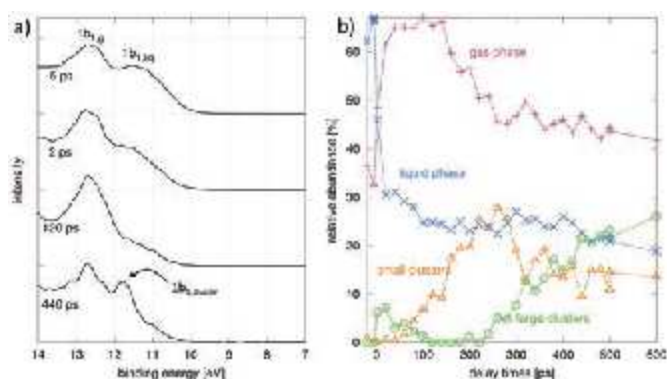


**Fig. 2:** a) Photoelectron spectra recorded at time-delays of 2 ps, 120 ps and 440 ps after the creation of a supercritical water phase by the pump-pulse. The spectrum at the top is a reference spectrum recorded at negative time-delays (-5 ps), and thus without excitation by the pump-pulse. b) During the expansion dynamics, the contribution of liquid water, gas phase and cluster signal to the photoelectron spectrum changes as a function of time. The newly developed multivariate method cTTF was used to extract the shown concentration profiles from the series of photoelectron spectra. Figures adapted from Ref. [6].

In the pump-probe experiments, the probe-pulse (25<sup>th</sup> harmonic, 38.7 eV) is used to record the photoelectron spectrum of the expanding hot phase at various points in time after energy deposition by the pump-pulse. Figure 2a) shows selected photoelectron spectra recorded at time-delays of 2 ps, 120 ps and 440 ps after excitation by the pump-pulse. Also shown is a spectrum at -5 ps, i.e. without excitation by the pump-pulse. This spectrum is the characteristic photoelectron signal of a liquid microjet for electron binding energies < 14 eV. It contains the photoelectron signal of the highest occupied molecular orbital (HOMO) in liquid water ( $1b_{1,liq}$ ) and in gaseous water ( $1b_{1,g}$ ) as well as some signal contribution from the HOMO-1 orbital at the high binding energy side of the spectrum. The spectra at 2 ps, 120 ps and 440 ps show how the expansion of the hot phase changes the photoelectron spectrum. As expected, the liquid signal decreases in intensity while the gas phase signal increases. Besides, the spectrum at 440 ps exhibits a new signal, which is located between gas phase and liquid phase signal, and which is consistent with the photoelectron spectrum of water clusters reported in the literature [22]. Furthermore, the position of the  $1b_{1,cluster}$  signal can be used to calculate the mean cluster size. The corresponding formula is given in Ref. [22]. In essence, the closer the  $1b_{1,cluster}$  signal is to the  $1b_{1,g}$  ( $1b_{1,liq}$ ) signal, the smaller (larger) the mean cluster size. For the quantitative evaluation of the entire series of spectra we have developed a multivariate method (cTTF) based on principle component analysis. Details are described in Ref. [6]. Therefore we assume that every photoelectron spectrum of the series of recorded pump-probe spectra is composed of the spectra of pure liquid water, water gas phase and water clusters. The cTTF algorithm then determines these pure component spectra and their contribution to every photoelectron spectrum of the series. This allows to obtain the concentration profiles shown in figure 2b). We note that the series of photoelectron spectra is satisfactorily represented when four pure components (liquid, gas and two cluster spectra) are taken into account, whereas three pure components (liquid, gas and one cluster spectrum) is not sufficient. In order to interpret the concentration profiles, we have simulated the expansion of supercritical water into vacuum with a simple fluid dynamics model, which is based on equations from expansion wave theory (see Ref. [6] for details). Important-

ly, this model delivers quantitative information on density and temperature in the expanding volume. This information together with the series of photoelectron spectra and the concentration profiles provide the following detailed mechanistic picture on the expansion of supercritical water into vacuum [6]: (figure 3)

(1) In our experiment vibrational excitation of water molecules by the pump-pulse (almost) instantaneously transfers the system into a supercritical state with a temperature of about 1000 K and a pressure above 1 GPa.

(2) This dense hot phase expands into vacuum on a picosecond timescale. Expansion goes along with a significant drop in density and temperature, in particular within the first few layers of water from which the major part of the photoelectron signal stems from. Within the first 5 ps of the expansion, density and temperature in this observation volume of our experiment drop to values around the critical point.

(3) From 5 ps to about 20 ps the volume further expands while temperature and density in the observation volume drop significantly below the critical values. In other words, a supersaturated phase emerges, in which condensation sets in and leads to the formation of small water clusters (~ 10 water molecules/cluster). (4) In the further course of the expansion ( $t > 150$  ps), the cluster size increases. Between 200 - 600 ps, the contribution of small clusters (~10 water molecules) decreases, while the signal from larger clusters (~50 water molecules) increases.

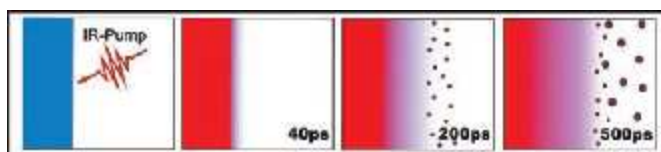


**Fig. 3:** This cartoon summarizes our findings on the ultrafast dynamics at the liquid water-vacuum interface after creation of a supercritical water phase by the pump-pulse [6]: Temperature and density of the first few nanometers of the expanding phase drop below the critical values within a few picoseconds. This results in a supersaturated phase, in which condensation seeds form and grow from small clusters to large clusters on a 100 ps timescale.

The uniqueness of this experiment can be seen in the combination of picosecond time-resolution, which allows to measure ultrafast dynamics, and the extremely high surface sensitivity. This enables to exclusively monitor the expansion mechanism within the first few layers of water, not concealed by expansion mechanisms proceeding in deeper water layers. Our results thus directly tie up to the numerous work on the initial sub-picosecond delocalization of molecular vibrations following vibrational excitation of liquid water, and connect this molecular scale picture of energy redistribution to research results on the macroscopic expansion of resulting highly excited thermodynamic water phases.

### 3. BINDING ENERGY OF SOLVATED ELECTRONS IN WATER

The hydrated electron  $e^-_{(aq)}$  is an electron solvated in water; much like ions are solvated by water molecules. Thereby the electron is on average surrounded by 6 water molecules, which form a cavity with a diameter of about 4 - 6 Å. Since their discovery by radiation chemists in 1962 [23], the hydrated electron is of enormous scientific interest. While the structure, energetics and dynamics of this species are of fundamental interest, its chemistry plays a role in research areas ranging

from DNA damage over atmospheric chemistry to electron-driven reactions in water-cooled nuclear reactors. Solvated electrons have therefore been investigated with various experimental techniques. While these experiments have revealed many properties of solvated electrons, one important information on solvated electrons remained inaccessible for experiments. This property was the binding energy of  $e^-_{(aq)}$ , the energy required to remove the electron from its solvation cavity and to completely separate it from the water. It is obvious that the binding energy is an important piece of information regarding stability, structure and reactivity of  $e^-_{(aq)}$ . The binding energy of  $e^-_{(aq)}$  has been inaccessible for a long time, because measuring it requires an experimental setup for time-resolved photoelectron spectroscopy on liquids. Time-resolution is required since solvated electrons in water are reactive and thus short lived species. This requires to create  $e^-_{(aq)}$  with the pump-pulse via ionization of a suitable precursor, and to record the photoelectron spectrum of  $e^-_{(aq)}$  with the probe-pulse. The binding energy of  $e^-_{(aq)}$  has for the first time been measured in 2008/2009 with the experimental setup described above, and results were published in 2010 [9]. In this experiment [9], we created solvated electrons in the liquid jet with a pump-pulse of 267 nm light via the charge-transfer-to-solvent (CTTS) excitation of the anionic complex  $[\text{Fe}(\text{CN})_6]^{4-}$  in solution. This complex has been selected because of its high charge, which warrants that it is fully solvated by water molecules. Further, the complex delivers solvated electrons in high quantum yield after excitation with 267 nm light. Time-delayed to the creation of  $e^-_{(aq)}$ , a high-harmonic probe-pulse (25<sup>th</sup> harmonic, 38.7 eV) is used to record the photoelectron spectrum of the system. Figure 4 shows the photoelectron spectrum recorded at a time delay of 100 ps. The signal centered at a binding energy of 3.3 eV is the photoelectron spectrum of the solvated electron in water. The signal at binding energies > 4.5 eV originates from the HOMO of the  $[\text{Fe}(\text{CN})_6]^{4-}$  complex. Signal intensities of  $e^-_{(aq)}$  are weak and require a careful analysis of the noise level. The right part of figure 4 shows the noise spectrum (red) which belongs to the photoelectron spectrum on the left side (orange). This noise spectrum is the part of the original time-of-flight spectrum

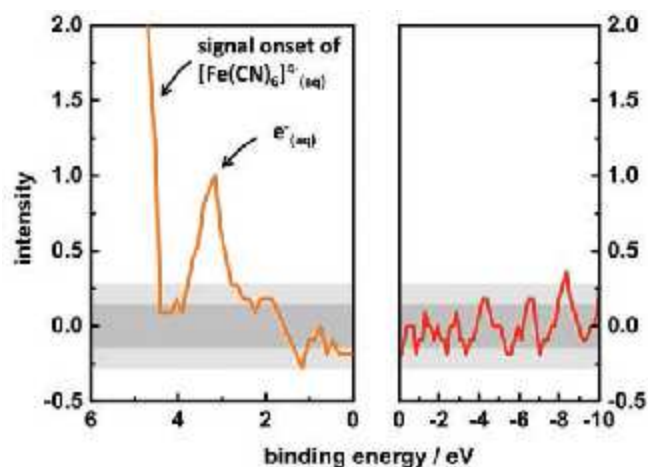


Fig. 4: The left part shows the photoelectron spectrum of the solvated electron recorded at a time-delay of 100 ps after the generation of hydrated electrons via the charge-transfer-to-solvent excitation of  $[\text{Fe}(\text{CN})_6]^{4-}$ . The noise (grey bands) is determined from the spectrum on the right (red line). See text for details.

which formally belongs to the negative binding energy range from -10 to 0 eV; a range in which no photoelectron signal from the sample can appear. The zero line is the mean value of the noise, while the dark grey band indicates  $\pm(1$  standard deviation) from this value. Assuming a normal distribution, the dark grey band includes 68.3 % of the noise. The light grey band represents  $\pm(2$  standard deviations) from the mean value and accordingly includes 95.4 % of the noise. Transferring this noise band to the photoelectron spectrum on the left side underlines the presence of a photoelectron signal at a binding energy of 3.3 eV.

In a second set of experiments the 267 nm pump-pulse generated solvated electrons via a two-photon ionization process of water molecules in a pure water sample. The photoelectron spectrum obtained in this experiment is shown in figure 5. It exhibits a signal at a binding energy of 1.6 eV. This signal is attributed to a solvated electron at the surface of water. This partially solvated electron must be a stable form of the solvated electron since its photoelectron signal has still been detected for time delays of 100 ps. With regard to this long lifetime we note that the temperature of the liquid jet surface is at about 0 °C or even below [7]. A supercooled water phase might thus be responsible for the stability of surface solvated electrons. Our hypothesis is that two-photon ionization of pure water leads to the formation of solvated electrons at the surface and in the bulk. However, due to the high surface sensitivity of photoelectron spectroscopy only the signal of the surface solvated electron is clearly present in the photoelectron spectrum. In contrast to this, in the experiment on the  $[\text{Fe}(\text{CN})_6]^{4-}$  solution mainly bulk solvated electrons are created and detected (figure 4). The reason is that the highly-charged  $[\text{Fe}(\text{CN})_6]^{4-}$  complex is fully solvated by water molecules, and thus mainly delivers bulk solvated electrons. In addition, in the experiment on the  $[\text{Fe}(\text{CN})_6]^{4-}$  complex, the intensity of the pump-pulse was held below the threshold for two-photon ionization. This warrants that solvated electrons are only created via photoionization of  $[\text{Fe}(\text{CN})_6]^{4-}$  and not via two-photon ionization of water molecules.

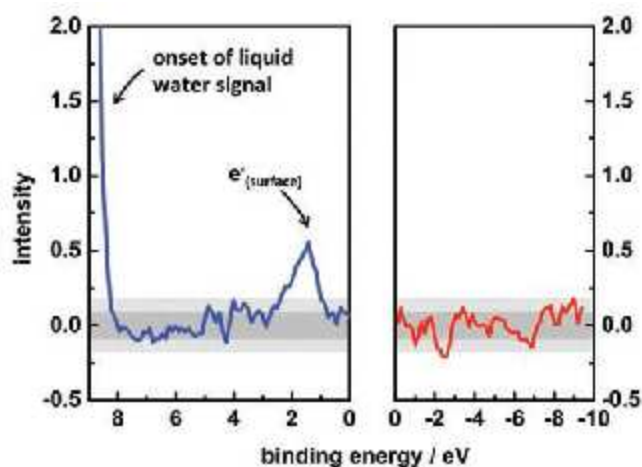


Fig. 5: The left part shows the photoelectron spectrum of a surface-solvated electron, generated via 2-photon ionization of water molecules by the 267 nm pump-pulse. The noise (grey bands) is determined from the spectrum on the right (red line). See text for details.

Unique to this experiment is that it allowed - for the first time - to measure the binding energy of the solvated electron in water ( $E_{\text{bind}}(e_{\text{aq}}^-) = 3.3$  eV). This result provides an important benchmark for theoretical studies and complements work on anionic water clusters, ice surfaces and transient absorption experiments in bulk liquids. Besides, detection of a stable surface solvated state of solvated electrons ( $E_{\text{bind}}(e_{\text{aq}}^-) = 1.6$  eV) was possible due to the high surface sensitivity of photoelectron spectroscopy. However, questions regarding formation, stability, local solvation environment and dynamics of surface solvated electrons are still to be answered.

## CONCLUSION

Picosecond time-resolved photoelectron spectroscopy on liquid microjets is a powerful tool to investigate fundamental phenomena and dynamics at the liquid water/vacuum interface. Key is that the surface sensitivity of photoelectron spectroscopy confines the experiment to the surface layer and the first few nanometers below. As demonstrated by the experiments presented above, this aspect renders it an exquisite and unique tool for the investigation of surface dynamics. Our current experiments are centered around surface active molecules and their ultrafast dynamics following excitation by light.

## REFERENCES

- [1] T. W. Kim, K. S. Choi, Nanoporous  $\text{BiVO}_4$  Photoanodes with Dual-Layer Oxygen Evolution Catalysts for Solar Water Splitting, *Science* **343**, 990 (2014).
- [2] F. Mayer, D. Wheatley, M. Hoppert, in *Water and the Cell* (Eds.: G. H. Pollack, I. L. Cameron, D. N. Wheatley), Springer, pp. 253, (2006).
- [3] E. M. Knipping, M. J. Lakin, K. L. Foster, P. Jungwirth, D. J. Tobias, R. B. Gerber, D. Dabdub, B. J. Finlayson-Pitts, Experiments and Simulations of Ion-Enhanced Interfacial Chemistry on Aqueous NaCl Aerosols, *Science* **288**, 301 (2000).
- [4] O. Link, E. Lugovoy, K. Siefertmann, Y. Liu, M. Faubel, B. Abel, Ultrafast Electronic Spectroscopy for Chemical Analysis near Liquid Water Interfaces: Concepts and Applications, *Appl. Phys.* **A 96**, 117 (2009).
- [5] M. Faubel, K. R. Siefertmann, Y. Liu, B. Abel, Ultrafast Soft X-Ray Photoelectron Spectroscopy at Liquid Water Microjets, *Acc. Chem. Res.* **45**, 120 (2011).
- [6] T. Gladysz, B. Abel, K. R. Siefertmann, Expansion Dynamics of Supercritical Water Probed by Picosecond Time-Resolved Photoelectron Spectroscopy, *Phys. Chem. Chem. Phys.* **17**, 4926 (2015).
- [7] E. Vöhlinger-Martinez, O. Link, E. Lugovoy, K. R. Siefertmann, F. Wiederschein, H. Grubmüller, B. Abel, Hydrogen Bond Dynamics of Superheated Water and Methanol by Ultrafast IR-Pump and EUV-Photoelectron Probe Spectroscopy, *Phys. Chem. Chem. Phys.* **16**, 19365 (2014).
- [8] O. Link, E. Vöhlinger-Martinez, E. Lugovoy, Y. X. Liu, K. Siefertmann, M. Faubel, H. Grubmüller, R. B. Gerber, Y. Miller, B. Abel, Ultrafast Phase Transitions in Metastable Water near Liquid Interfaces, *Faraday Discuss.* **141**, 67 (2009).
- [9] K. R. Siefertmann, Y. Liu, E. Lugovoy, O. Link, M. Faubel, U. Buck, B. Winter, B. Abel, Binding Energies, Lifetimes and Implications of Bulk and Interface Solvated Electrons in Water, *Nat. Chem.* **2**, 274 (2010).
- [10] K. R. Siefertmann, B. Abel, The Hydrated Electron: A Seemingly Familiar Chemical and Biological Transient, *Angew. Chem. Int. Ed.* **50**, 5264 (2011).
- [11] J. Stähler, J.-C. Deinert, D. Wegkamp, S. Hagen, M. Wolf, Real-Time Measurement of the Vertical Binding Energy During the Birth of a Solvated Electron, *J. Am. Chem. Soc.* Article ASAP, DOI: 10.1021/ja511571y (2015).
- [12] M. H. Elkins, H. L. Williams, A. T. Shreve, D. M. Neumark, Relaxation Mechanism of the Hydrated Electron, *Science* **342**, 1496 (2013).
- [13] K. R. Siefertmann, C. D. Pemmaraju, S. Nepl, A. Shavorskiy, A. A. Cordones, J. Vura-Weis, D. S. Slaughter, F. P. Sturm, F. Weise et al., Atomic-Scale Perspective of Ultrafast Charge Transfer at a Dye-Semiconductor Interface, *J. Phys. Chem. Lett.* **5**, 2753 (2014).
- [14] L. Nugent-Glandorf, M. Scheer, D. A. Samuels, A. M. Mulhisen, E. R. Grant, X. M. Yang, V. M. Bierbaum, S. R. Leone, Ultrafast Time-Resolved Soft X-Ray Photoelectron Spectroscopy of Dissociating  $\text{Br}_2$ , *Phys. Rev. Lett.* **87**, 193002 (2001).
- [15] F. Krausz, M. Ivanov, Attosecond Physics, *Rev. Mod. Phys.* **81**, 163 (2009).
- [16] M. Faubel, T. Kisters, Non-Equilibrium Molecular Evaporation of Carboxylic Acid Dimers, *Nature* **339**, 527 (1989).
- [17] B. Winter, R. Weber, W. Widdra, M. Dittmar, M. Faubel, I. V. Hertel, Full Valence Band Photoemission from Liquid Water Using EUV Synchrotron Radiation, *J. Phys. Chem.* **A 108**, 2625 (2004).
- [18] B. Winter, M. Faubel, Photoemission from Liquid Aqueous Solutions, *Chem. Rev.* **106**, 1176 (2006).
- [19] Y. I. Suzuki, K. Nishizawa, N. Kurahashi, T. Suzuki, Effective Attenuation Length of an Electron in Liquid Water between 10 and 600 eV, *Phys. Rev.* **E 90**, 010302 (2014).
- [20] S. Thürmer, R. Seidel, M. Faubel, W. Eberhardt, J. C. Hemminger, S. E. Bradforth, B. Winter, Photoelectron Angular Distributions from Liquid Water: Effects of Electron Scattering, *Phys. Rev. Lett.* **111**, 173005 (2013).
- [21] I.-F. W. Kuo, C. J. Mundy, An Ab Initio Molecular Dynamics Study of the Aqueous Liquid-Vapor Interface, *Science* **303**, 658 (2004).
- [22] S. Barth, M. Oncak, V. Ulrich, M. Mucke, T. Lischke, P. Slavicek, U. Hergenbahn, Valence Ionization of Water Clusters: From Isolated Molecules to Bulk, *J. Phys. Chem.* **A 113**, 13519 (2009).
- [23] E. J. Hart, J. W. Boag, Absorption Spectrum of Hydrated Electron in Water and in Aqueous Solutions, *J. Am. Chem. Soc.* **84**, 4090 (1962).